Role of Amine Functionality for CO_2 Chemisorption on Silica

SUPPORTING INFORMATION

M. W. Hahn, J. Jelic, E. Berger, K. Reuter, A. Jentys*, J. A. Lercher*
Department of Chemistry, Catalysis Research Center
Technische Universität München
Lichtenbergstraße 4, 85747 Garching, Germany
E-mail: johannes.lercher@mytum.de, jentys@mytum.de

A. Experimental

Chemicals

Phenyltrimethoxysilane (PTMS, purity ≥ 97 %), (3-aminopropyl)trimethoxysilane (APTMS, purity ≥ 97 %), trimethoxy[3-(methylamino)propyl]silane (MAPS, purity ≥ 97 %), N-[3-(trimethoxysilyl)propyl]ethylenediamine (AAMS, purity ≥ 97 %) and benzyl alcohol (purity ≥ 99 %) were purchased from Sigma Aldrich. Tetraethylorthosilicate (TEOS) and the copolymer Pluronic RPE 1740 were provided by WACKER and BASF, respectively. All chemicals were used without any additional purification. The reactor column was filled with deionized (DI) water.

X-Ray Diffraction

Powder X-ray diffraction (XRD) patterns were measured on a Philips X'pert diffractometer with an X'celerator detector (Cu Kα radiation). All diffractograms were measured with a step size of 0.033° in the range of $2\Theta = 5$ to 40°.

N_2 Physisorption

All sorbents were outgassed under vacuum at 100 °C for 1 h. The Brunauer-Emmett-Teller (BET) method[1] was applied to quantify the surface area. The mesopore volume (pore size: 2 – 50 nm) and pore size distribution were calculated by the Barrett-Joyner-Halenda (BJH) model (desorption branch of the isotherm).[2]

Scanning electron microscopy (SEM).

SEM images of calcined adsorbents were recorded on a FEI Helios NanoLab 660 Focused Ion Beam (DualBeam FIB) microscope. SEM images of non-calcined sorbents were recorded with a Jeol JSM 7500F. All images were taken by secondary electron imaging (SEI) at 2 kV of non-sputtered adsorbents

Adsorption-desorption experiments

The adsorption and desorption steps (concentration swing with N_2) were carried out for 180 min at constant temperatures of 50 and 75 °C in a Setaram Sensys Evo, respectively. Additionally, adsorption was carried out for 3 h at 50 °C under atmospheric flow conditions (10 vol.% CO_2 in N_2) followed by a 3 h desorption section in pure N_2 at 75 °C for 10 times to obtain a set of multi-cycle experiments.

B. Structural Properties of the Sorbents for Different Aminosilanes

The surface properties of SiO_2 spheres strongly depend on the method chosen for the removal of the surfactants (e.g., Soxhlet extraction or calcination). The functionality and the concentration of amines, employed in the synthesis, influence the morphology of the sorbents through base catalyzed condensation of TEOS.[3] The content of amine groups, for all sorbents discussed in this section, was kept constant at 3.3 mmol g^{-1} to ensure comparability among the sorbents and to solely focus on the impact of different amine functionalities during synthesis. The effect of different amine concentrations on sorbent characteristics like surface area and pore volume is discussed in section C.

The X-ray diffraction patterns (XRD) of non-calcined APTMS(1), MAPS(2) and AAMS(1,2) are depicted in Figure S1A. The diffraction pattern did not show any distinct changes prior or upon calcination of the sorbents at 500 °C in synthetic air (Figure S1B). Thus, no defined crystalline structure could be observed by XRD for all SiO_2 spheres and therefore, a well-defined long range order was excluded (Figure S1).

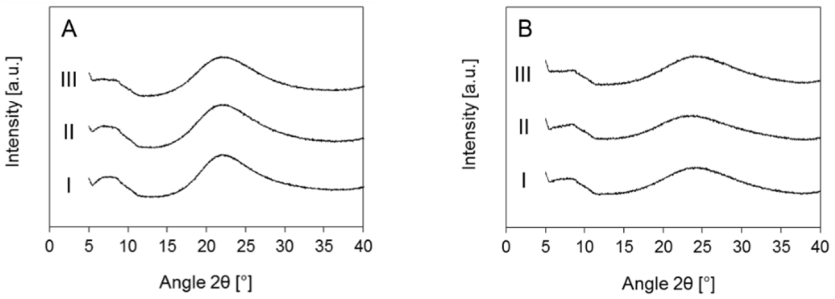

Figure S1. XRD of (I) APTMS(1) with 3.31 mmol N/g, (II) MAPS(2) with 3.30 mmol N/g and (III) AAMS(1,2) with 3.29 mmol N/g. Intensity in arbitrary units.

The concentration of residual surfactants in the adsorbents after Soxhlet extraction was below 1 mol % based on the content of aminosilanes for APTMS(1), MAPS(2) and AAMS(1,2). The N_2 physisorption isotherms of mesoporous SiO_2 spheres (3.3 – 3.6 mmol g^{-1}) as well as the pore size distributions are displayed in Figure S2. The pore volume was most pronounced for APTMS(1) and AAMS(1,2) that also exhibited the highest surface areas with 82 and 92 m^2 g^{-1}, respectively (Table S1). The surface area and pore volume of MAPS(2) was approximately 50 % lower compared to APTMS(1). The sorbents revealed a hierarchical distribution of the pores independent of the aminosilane employed in the synthesis (Figure S2A). The hierarchical structure of the sorbents has been confirmed in our former studies by scanning electron microscopy (SEM) and is also displayed in Figure S3A.[3-5] The pore size

distribution was well-defined for APTMS(1) and AAMS(1,2) with average pore sizes at around 15 and 30 nm, respectively. In contrast, a broader distribution was observed for MAPS(2) (Figure S3B).

Table S1. Amine concentration, BET surface area and pore volume determined by N_2 physisorption of SiO_2 spheres. Mesopore volume determined by BJH method (desorption branch).

	Amine concentration [mmol g^{-1}]	BET surface area [m^2 g^{-1}]	Mesopore volume [cm^3 g^{-1}]
APTMS(1)	3.31	82	0.27
MAPS(2)	3.30	40	0.13
AAMS(1,2)	3.29	92	0.41

The pK_a values, representing the Brønsted basicity, of primary and secondary amines are both between 10 and 11.[6-7] Secondary amines reveal a higher Lewis basicity because of an enhanced electron density, induced by the additional alkyl group neighboring the N atom.[7-8] Thus, we calculated the proton affinity, an intrinsic property of the employed amines that is independent of the solvent used. The proton affinity reflects the acidity of a molecule comparable to a pK_a value that is, however, dependent on the reaction medium. The proton affinity determined by DFT was 30 and 43 kJ mol^{-1} higher for secondary amines in MAPS(2) and AAMS(1,2) than for APTMS(1) as displayed in Table S1.

Table S2. Proton affinity of primary, secondary and bifunctional aminosilanes determined by DFT.

Proton affinity (kJ mol^{-1})			
APTMS(1)	MAPS(2)	AAMS(1,2)	
		Primary	Secondary
- 916	- 946	- 917	- 959

The base catalyzed condensation of TEOS was faster when secondary aminosilanes were employed in the synthesis due to their higher nucleophilicity.[9] Thus, the enhanced condensation rate of TEOS with MAPS(2) led to cross-linking and a bulky and less-defined SiO_2 framework (Figure S2C, Figure S3B). In agreement with the latter, the most ordered structure of all sorbents was achieved by the primary aminosilane, being the weakest Lewis base (Figure S2B, Figure S3B). Furthermore, the high mesopore volume of SiO_2 spheres synthesized with AAMS(1,2) is attributed to the enhanced length of the aminosilane, directing the structural alignment of the condensed TEOS molecules (Table S1, Figure S2D, Figure S3B).

In summary, the structural properties of SiO_2 spheres were least evolved when synthesized with the strong secondary Lewis base MAPS(2) compared to APTMS(1) and AAMS(1,2).

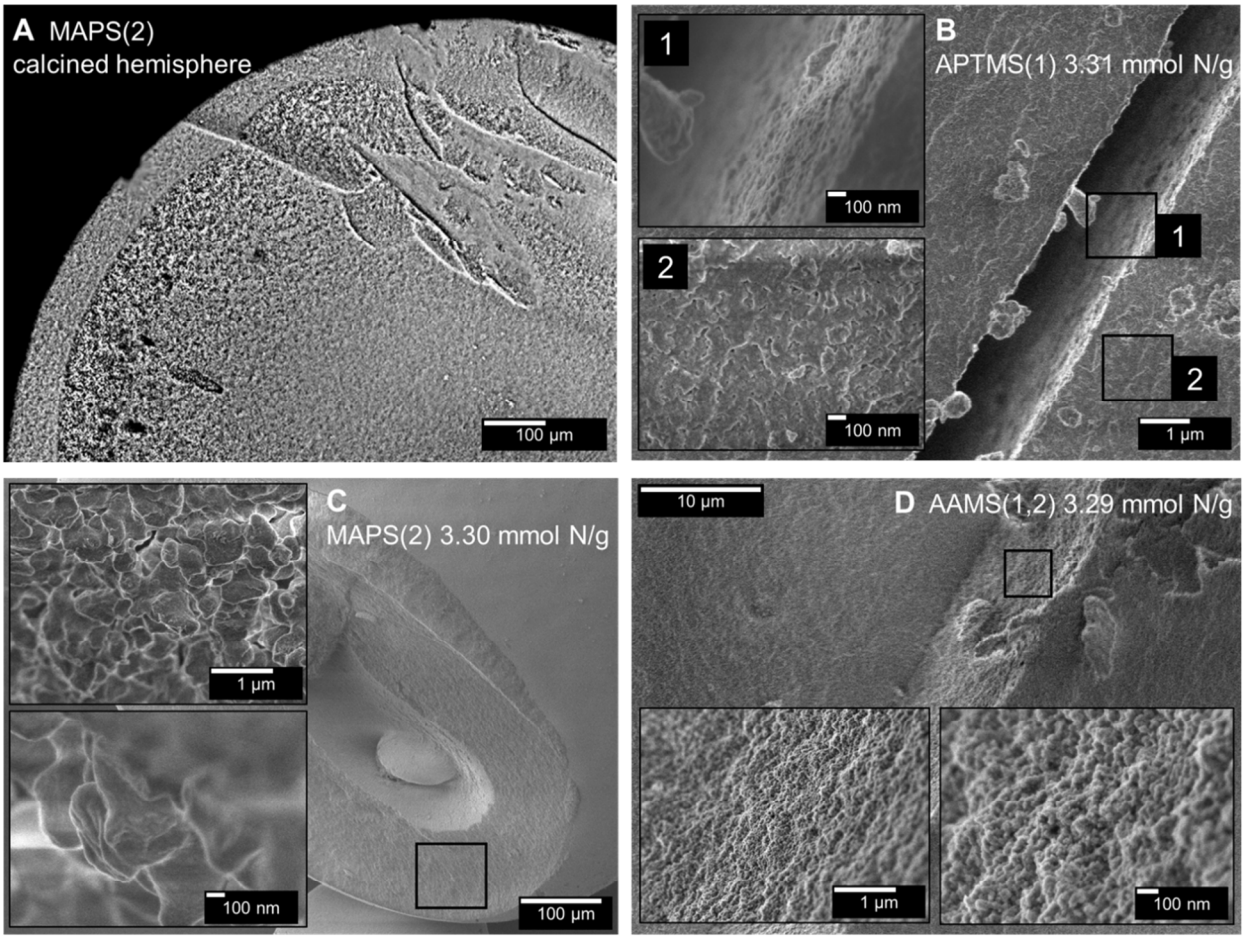

Figure S2. SEM images of the hierarchical structure of a (A) calcined hemisphere. Inner structure of (B) APTMS(1), (C) MAPS(2) and (D) AAMS(1,2).

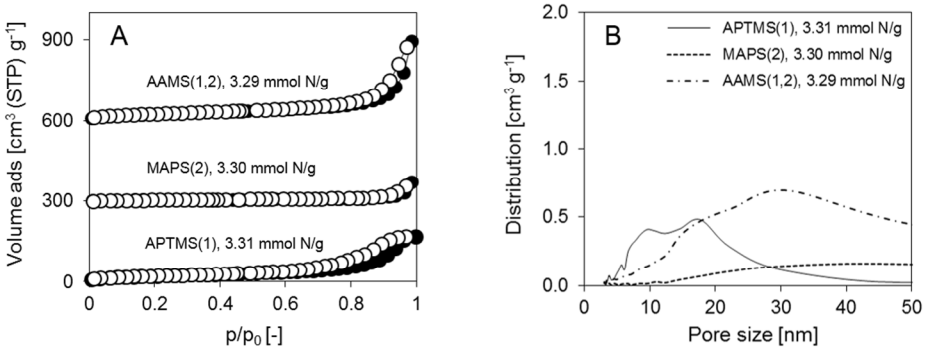

Figure S3. (A) Isotherms, adsorption (filled symbols) and desorption branches (unfilled symbols), wherein an offset of 300 is added between the isotherms of the various sorbents. (B) Pore size distribution (BJH method, desorption branch) of APTMS(1), MAPS(2) and AAMS(1,2) (Table S 1) determined by N_2 physisorption.

C. Structural Properties of the Sorbents for Different Amine Contents

The dependency of the surface area and pore volume of the sorbents on the amine contents is depicted in Figure S4. The maximum accessible surface area of 280 and 245 $m^2 g^{-1}$ was observed for monofunctional aminosilanes APTMS(1) and MAPS(2) with the lowest amine concentration. SiO_2 spheres synthesized with monofunctional amines exhibited a strong decline in the surface area and pore volume with increasing amine contents. As noted earlier, the amine content is eminent for the base catalyzed hydrolysis of the structure building silanes (e.g. TEOS), but also led to a decrease of surface area due to occupation of accessible sites by the aminosilanes itself. Thus, an optimum in the surface properties is anticipated and could be observed for the bibasic aminosilane AAMS(1,2) (Figure S4). The reduced hydrolysis rate in AAMS(1,2) due to sterical hindrance by pre-condensed silanes surrounding the aminosilane resulted in a trend that is proposed to occur for monofunctional aminosilanes at lower amine concentrations.

Low concentrations of especially monofunctional amines (APTMS(1) and MAPS(2)) result in high surface areas (> 200 $m^2 g^{-1}$) that exhibit a higher number of free physisorption sites for the adsorption of CO_2. At higher amine loadings chemisorption becomes the dominant form of adsorption due to reduced number of accessible Si-OH sites.

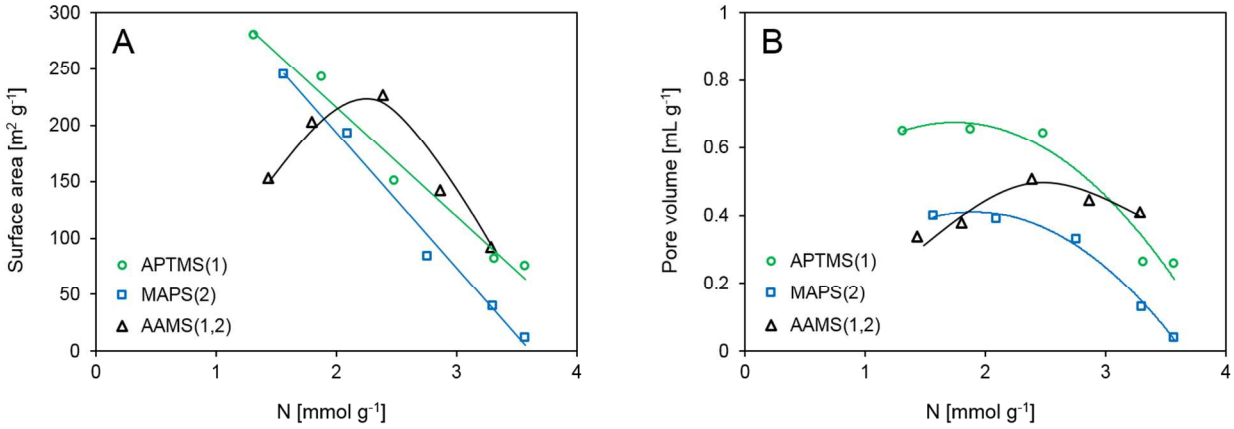

Figure S4. (A) Surface area and (B) pore volume of APTMS(1), MAPS(2) and AAMS(1,2) for various amine contents.

D. Adsorption-Desorption Properties and Long Term Cycle Stability

The long-term stability of an amine functionalized adsorbent is strongly influenced by the level of flue gas contamination (SO_x, NO_x, H_2O etc.) and the desorption conditions applied. Sayari reported that secondary amines exhibit a higher resistance against thermal degradation, i.e., formation of urea, compared to primary amines when H_2O is absent in the adsorption process.[10] The gaseous H_2O content in industrial flue gas streams (up to 15 vol.-%) hinders thermal degradation via hydrolysis independent of the amine functionality.[11] The amine content of the sorbents for long term studies was selected to yield the highest CO_2 uptake capacities as illustrated in Figure 4.

10 adsorption-desorption cycles were conducted for each adsorbent (Figure S6). The CO_2 uptake normalized to the amine concentration, i.e. the amine efficiency, remained constant over 10 cycles and was approximately 20 % for APTMS(1), 25 % for MAPS(2) and 10 % for AAMS(1,2). In summary, the amine functionalized SiO_2 spheres achieve excellent adsorption-desorption long-term properties for all employed aminosilane even without the presence of H_2O.

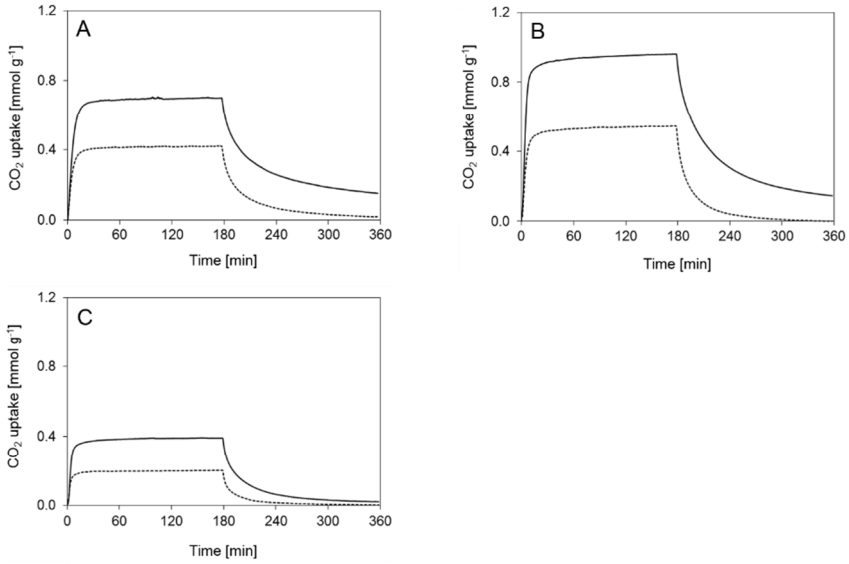

Figure S5. CO_2 adsorption of (A) APTMS(1) with 3.31 mmol N/g, (B) MAPS(2) with 3.57 mmol N/g and (C) AAMS(1,2) with 3.29 mmol N/g. Adsorption for 180 min under atmospheric flow conditions (50 °C, 10 vol.% CO_2 in N_2) followed by a 180 min desorption section in pure N_2. Constant adsorption-desorption temperature of 50 °C (solid line) and 75 °C (dotted line).

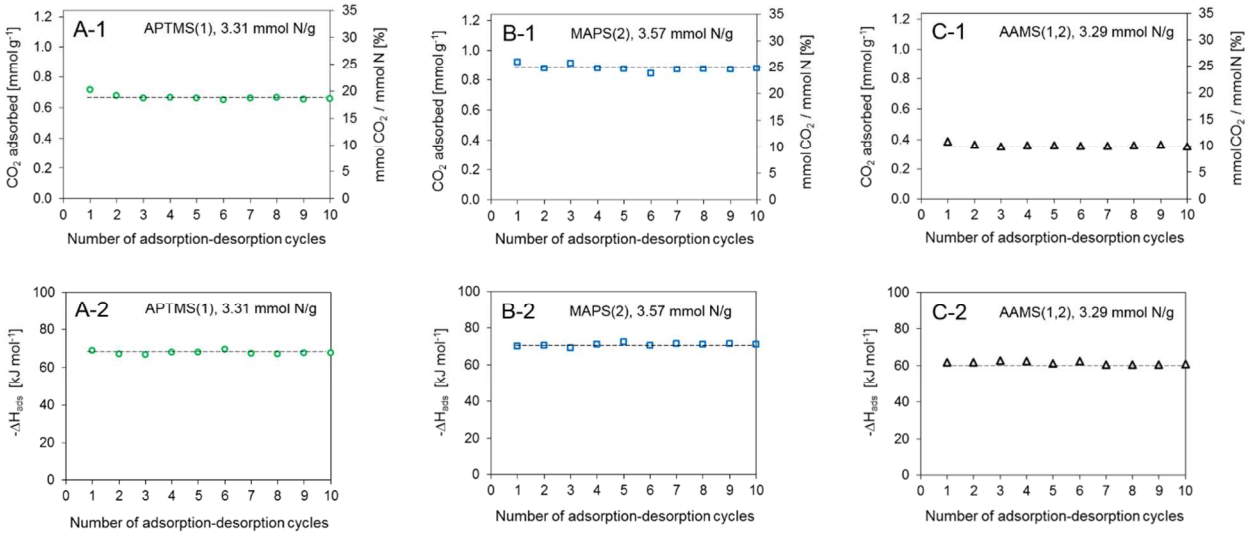

Figure S6. Temperature-swing multi-cycle CO_2 adsorption of (A) APTMS(1), (B) MAPS(2) and (C) AAMS(1,2) over 10 cycles. Values determined by TGA DSC under atmospheric flow conditions (50 °C, 10 vol.% CO_2 in N_2) and desorption at 75 °C in a flow of pure N_2. (1) Adsorbed CO_2 and (2) heats of adsorption.

E. Effect of the Amine Concentration on the Amine Efficiency and Heats of Adsorption

In order to quantify the impact of the physisorption of CO_2 on the pure SiO_2 support on the capture capability of the amine functionalized adsorbents the sorbents have been calcined and the adsorption capacity was obtained (Table S3). The calcination was carried out in synthetic air (100 mL min^{-1}) at 600 °C for 6 h with a heating rate of 2 °C min^{-1} to ensure the total removal of all remaining organic compounds. The uptake of the sorbents without amine groups present was in the order of 0.04 mmol g^{-1} (AAMS(1,2)) to 0.1 mmol g^{-1} (Table S3). Please note that the degree of physisorption is strongly dependent on the accessible surface area, which was higher for calcined SiO_2 spheres (>500 m^2 g^{-1}) compared to amine containing SiO_2 spheres (Figure S4). However, physisorption of CO_2 on the silanol surfaces cannot be excluded especially for amine loadings below 2 mmol g^{-1} (Figure S4).

Table S3. Amount of adsorbed CO_2 and heats of adsorption of CO_2 on calcined APTMS(1), MAPS(2) and AAMS(1,2) determined by TGA under flow conditions (quasi equilibrium). The amine contents before calcination: APTMS(1), 3.31 mmol N/g; (II) MAPS(2), 3.57 mmol N/g and AAMS(1,2), 3.29 mmol N/g

	CO_2 adsorbed [mmol g^{-1}]	- ΔH_{ads} [kJ mol^{-1}]
APTMS(1)_calcined	0.10	28
MAPS(2)_calcined	0.07	23
AAMS(1,2)_calcined	0.04	24

The CO_2 uptake normalized to the amine concentration (amine efficiency) and the heats of adsorption are illustrated in Figure S7. The amine efficiency of APTMS(1), MAPS(2) and AAMS(1,2) at an amine loading of 3.3 mmol g^{-1} were 23 %, 21 % and 12 %, respectively. As discussed above, the functionality of amines determines their maximum efficiency, i.e., 50 % for APTMS(1) and MAPS(2) and only 25 % for AAMS(1,2). However, encapsulation of aminosilanes in the SiO_2 network by condensation reactions in the base catalyzed synthesis significantly decreases the achievable amine efficiency by inaccessible amine sites of approximately 1.5 - 2 mmol g^{-1} (Figure S7). Thus, at low (below 10 %) amine concentrations the apparent amine efficiency significantly decreased to 5 – 6 % independent of the employed aminosilanes (Figure S7). The low heats of adsorption at low amine loadings (- 40 kJ mol^{-1}) are tentatively also correlated to the partial occlusion of the amine sites. The heats of adsorption steadily increased for higher amine concentrations from - 40 kJ mol^{-1} up to approximately - 75 kJ mol^{-1} except for APTMS(1) with the highest amine loading.

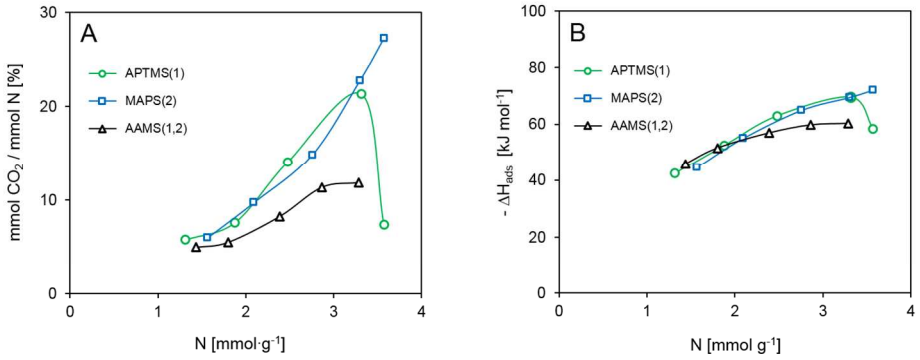

Figure S7. (A) Amine efficiency and (B) heats of adsorption versus the amine concentration. Values determined by TGA DSC under flow conditions at 50 °C.

F. Illustrations of the CO_2 Adsorption Mechanism

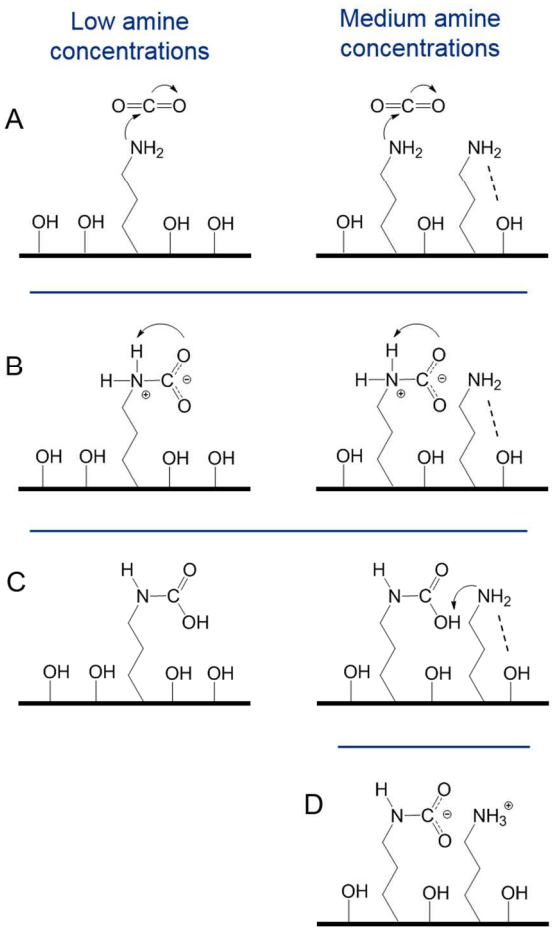

Figure S8. Potential adsorption structures formed by interactions of CO_2 and APTMS(1) at low and medium amine densities. (A) amine before adsorption, formation of a (B) zwitterion, (C) carbamic acid and an (D) ammonium carbamate.

G. IR Spectra and Peak Assignment

The IR spectra of CO_2 adsorbed on SiO_2 spheres functionalized with APTMS(1), MAPS(2), AAMS(1,2) are displayed in Figure S9. The spectra of CO_2 on APTMS(1) and AAMS(1,2) exhibited only a weakly defined band around 1690 cm^{-1} characteristic for C=O stretching vibration in carbamic acid (Figure S9). The corresponding OH deformation band at 1380 cm^{-1} was weak with APTMS(1) and not observable for AAMS(1,2) (Figure S9).[12-13]

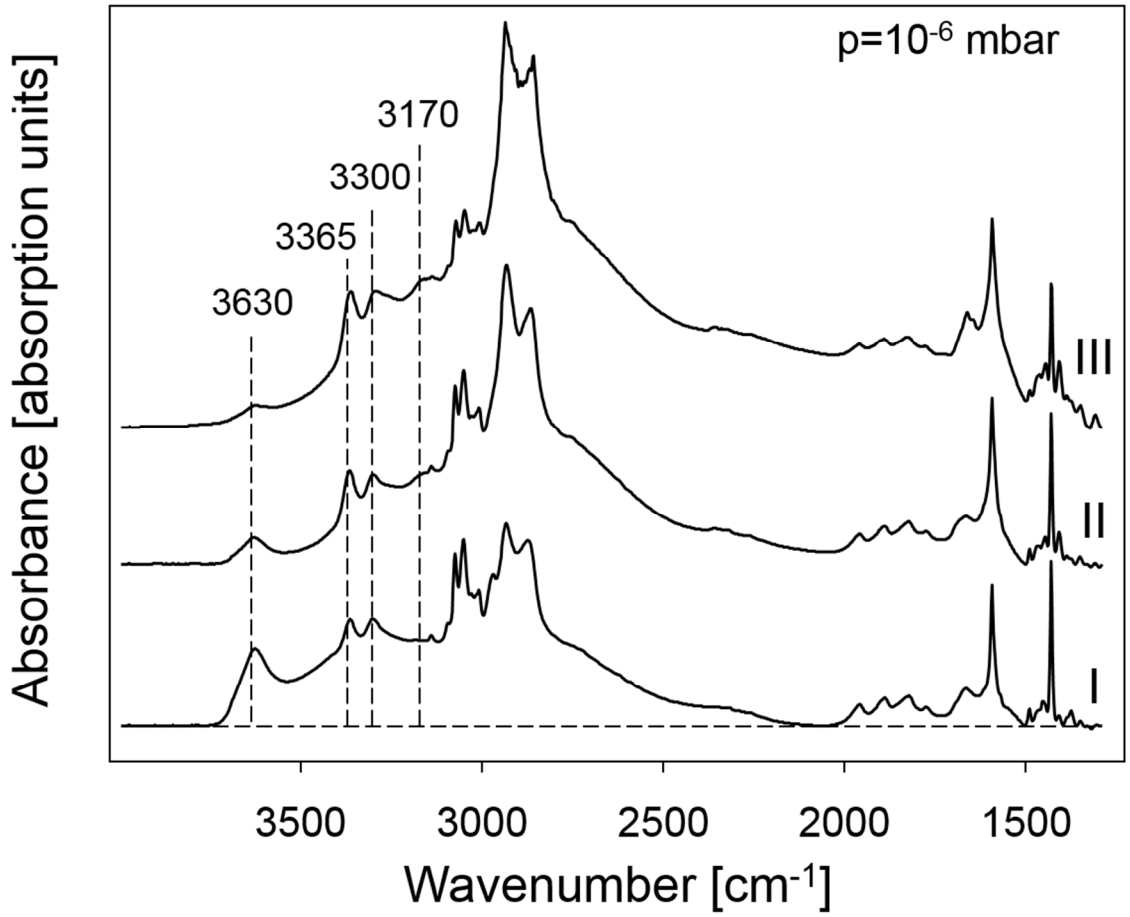

Figure S9. Intensity of surface Si-OH groups (3630 cm^{-1}) as a function of the concentration of amines groups. IR spectra of APTMS(1) with an amine content of (I) 1.31 (II) 2.48 and (III) 3.57 mmol N/g. Spectrum range from 3500 - 1250 cm^{-1}.

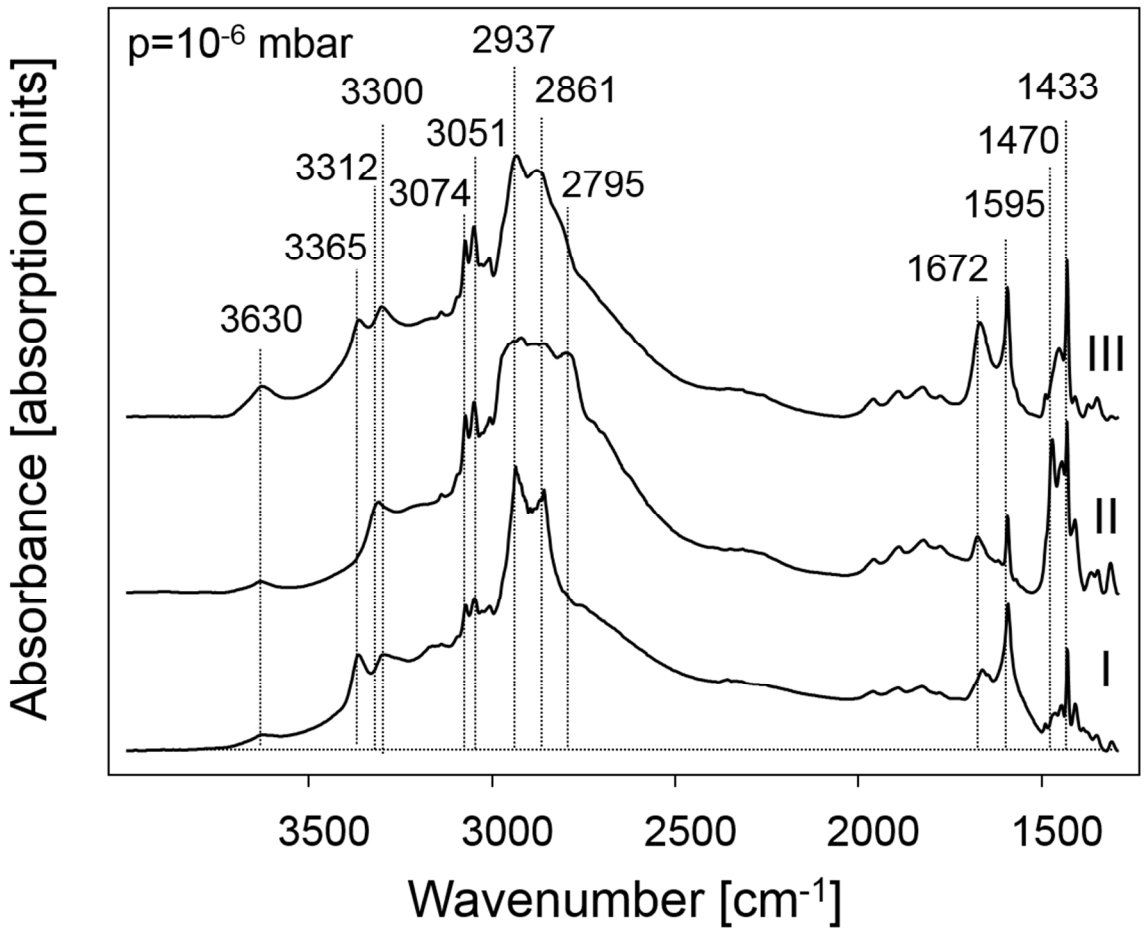

Figure S10. IR spectra of (I) APTMS(1) with 3.57 mmol N/g, (II) MAPS(2) with 3.57 mmol N/g) and (III) AAMS(1,2) with 3.29 mmol N/g. Spectrum range from 3500 – 1250 cm^{-1}

Table S4. Overview of IR bands present on amine functionalized SiO_2 supports.

Wavenumber [cm^{-1}]	Assignment	References
>3750	OH stretching vibration of free silanol groups (support)	14-16
3700 - 3000	OH stretching of hydrogen bonded OH groups (H_2O)	14, 17
3650 - 3630	OH stretching of hydrogen bonded OH groups (support)	14, 18-19
3370 - 3360	*Asymmetric* NH_2-stretching vibration of primary amines	10, 18, 20
3330 - 3300	*Symmetric* NH_2 stretching vibration of primary amines	10, 18-19, 21
	NH stretching vibration of secondary amines	
3090 - 3010	CH stretching vibration in aromatics	22-23
3000 - 2980	NH stretching vibration (protonation by Si-OH)	12
2930 - 2850	CH_2 stretching vibration	18-19, 21
2820 - 2760	NCH_3 stretching vibration	24
1670 - 1620	*Asymmetric* NH_x^+ deformation (protonation by Si-OH)	15, 19, 22
1640 - 1600	NH_x deformation (variation by degree of H-bonding)	10, 14, 18-20
1490 - 1480	*Symmetric* NH_x^+ deformation (protonation by Si-OH)	19-20, 22
1470 - 1440	CH_2 bending	14, 19, 21, 25
1440 - 1410	CN stretching	19, 21, 25-26

Table S5. IR bands formed during adsorption of CO_2 on amine functionalized SiO_2 supports.

Wavenumber [cm^{-1}]	Assignment	References
3615, 3715	Combination bands of gas phase CO_2	19, 27
3440 - 3420	NH stretching vibration (carbamates, carbamic acid)	14, 20, 28
3000	Stretching vibration of COOH (carbamic acid, broad peak)	22, 29
2345	Gas phase CO_2	20, 30
	Asymmetric stretching of linearly physisorbed CO_2	
1720 - 1670	CO stretching vibration (carbamic acid)	12-14, 18
1670 - 1620	*Asymmetric* NH_x^+ deformation	15, 19, 22
1565 - 1550	*Asymmetric* COO^- stretching vibration (ammonium carbamate)	14, 16, 20, 28
1490 - 1480	*Symmetric* NH_x^+ deformation	19-20, 22
1430 - 1400	*Symmetric* COO^- stretching (ammonium carbamate)	19-20, 22
1380	OH deformation (carbamic acid)	12-13
1330 - 1300	NCOO skeletal vibration	16, 18, 28

H. Supporting References

1. Brunauer, S.; Emmett, P. H.; Teller, E., Adsorption of Gases in Multimolecular Layers. *J Am Chem Soc* **1938**, *60*, 309-319.
2. Barrett, E. P.; Joyner, L. G.; Halenda, P. P., The Determination of Pore Volume and Area Distributions in Porous Substances. I. Computations from Nitrogen Isotherms. *J Am Chem Soc* **1951**, *73*, 373-380.
3. Hahn, M. W.; Steib, M.; Jentys, A.; Lercher, J. A., Tailoring Hierarchically Structured SiO_2 Spheres for High Pressure CO_2 Adsorption. *J Mater Chem A* **2014**, *2*, 13624-13634.
4. Scholz, S.; Lercher, J. A., Hierarchically Structured Millimeter-Sized (Organo) Silica Spheres with a Macroporous Shell and a Meso/Microporous Core. *Chem Mater* **2011**, *23*, 2091-2099.
5. Scholz, S.; Bare, S. R.; Kelly, S. D.; Lercher, J. A., Controlled One-Step Synthesis of Hierarchically Structured Macroscopic Silica Spheres. *Micropor Mesopor Mat* **2011**, *146*, 18-27.
6. Hall Jr, H., Correlation of the Nucleophilic Reactivity of Aliphatic Amines. *J Org Chem* **1964**, *29*, 3539-3544.
7. Hall, H. K., Correlation of the Base Strengths of Amines1. *J Am Chem Soc* **1957**, *79*, 5441-5444.
8. Ripin, D. H.; Evans, D. A., PK_a's of CH Bonds at Heteroatom Substituted Carbon & References. 2014.
9. Brotzel, F.; Chu, Y. C.; Mayr, H., Nucleophilicities of Primary and Secondary Amines in Water. *J Org Chem* **2007**, *72*, 3679-3688.
10. Sayari, A.; Heydari-Gorji, A.; Yang, Y., CO_2-Induced Degradation of Amine-Containing Adsorbents: Reaction Products and Pathways. *J Am Chem Soc* **2012**, *134*, 13834-13842.
11. Sayari, A.; Belmabkhout, Y., Stabilization of Amine-Containing CO_2 Adsorbents: Dramatic Effect of Water Vapor. *J Am Chem Soc* **2010**, *132*, 6312-6314.
12. Bossa, J. B.; Borget, F.; Duvernay, F.; Theule, P.; Chiavassa, T., Formation of Neutral Methylcarbamic Acid ($CH_3NHCOOH$) and Methylammonium Methylcarbamate [$CH_3NH_3^+$][$CH_3NHCO_2^-$] at Low Temperature. *J Phys Chem A* **2008**, *112*, 5113-5120.
13. Bossa, J. B.; Theule, P.; Duvernay, F.; Borget, F.; Chiavassa, T., Carbamic Acid and Carbamate Formation in NH_3:CO_2 Ices-Uv Irradiation Versus Thermal Processes. *Astron Astrophys* **2008**, *492*, 719-724.
14. Knöfel, C.; Martin, C.; Hornebecq, V.; Llewellyn, P. L., Study of Carbon Dioxide Adsorption on Mesoporous Aminopropylsilane-Functionalized Silica and Titania Combining Microcalorimetry and In Situ Infrared Spectroscopy. *J Phys Chem C* **2009**, *113*, 21726-21734.
15. Hiyoshi, N.; Yogo, K.; Yashima, T., Adsorption Characteristics of Carbon Dioxide on Organically Functionalized SBA-15. *Micropor Mesopor Mat* **2005**, *84*, 357-365.
16. Huang, H. Y.; Yang, R. T.; Chinn, D.; Munson, C. L., Amine-Grafted MCM-48 and Silica Xerogel as Superior Sorbents for Acidic Gas Removal from Natural Gas. *Ind Eng Chem Res* **2003**, *42*, 2427-2433.
17. Tanaka, K.; White, J. M., Characterization of Species Adsorbed on Oxidized and Reduced Anatase. *J Phys Chem* **1982**, *86*, 4708-4714.
18. Tanthana, J.; Chuang, S. S. C., In Situ Infrared Study of the Role of PEG in Stabilizing Silica-Supported Amines for CO_2 Capture. *Chemsuschem* **2010**, *3*, 957-964.
19. Danon, A.; Stair, P. C.; Weitz, E., FTIR Study of CO_2 Adsorption on Amine-Grafted SBA-15: Elucidation of Adsorbed Species. *J Phys Chem C* **2011**, *115*, 11540-11549.

20. Bacsik, Z.; Ahlsten, N.; Ziadi, A.; Zhao, G. Y.; Garcia-Bennett, A. E.; Martin-Matute, B.; Hedin, N., Mechanisms and Kinetics for Sorption of CO_2 on Bicontinuous Mesoporous Silica Modified with N-Propylamine. *Langmuir* **2011**, *27*, 11118-11128.
21. Srikanth, C. S.; Chuang, S. S. C., Spectroscopic Investigation into Oxidative Degradation of Silica-Supported Amine Sorbents for CO_2 Capture. *Chemsuschem* **2012**, *5*, 1435-1442.
22. Colthup, N. B.; Daly, L. H.; Wiberly, S. E., *Introduction to Infrared and Raman Spectroscopy*; Academic press: San Diego, 1990; Vol. Third Edition.
23. Akalin, E.; Akyüz, S., Force Field and IR Intensity Calculations of Aniline and Transition Metal (Ii) Aniline Complexes. *J Mol Struct* **1999**, *482*, 175-181.
24. Schwetlick, K., *Organikum*; Wiley VCH: Weinheim, 2009; Vol. 23.
25. Socrates, G., *Infrared and Raman Characteristic Group Frequencies: Tables and Charts*; Wiley: Chichester, New York, 2001; Vol. 3rd Edition.
26. Langer, J.; Schrader, B.; Bastian, V.; Jacob, E., Infrared-Spectra and Force-Constants of Urea in the Gaseous-Phase. *Fresen J Anal Chem* **1995**, *352*, 489-495.
27. Herzberg, G., *Infrared and Raman Spectra*; Van Nostrand: New York, **1945**.
28. Wang, X. X.; Schwartz, V.; Clark, J. C.; Ma, X. L.; Overbury, S. H.; Xu, X. C.; Song, C. S., Infrared Study of CO_2 Sorption over "Molecular Basket" Sorbent Consisting of Polyethylenimine-Modified Mesoporous Molecular Sieve. *J Phys Chem C* **2009**, *113*, 7260-7268.
29. Khanna, R.; Moore, M., Carbamic Acid: Molecular Structure and IR Spectra. *Spectrochim Acta Mol Biomol Spectros* **1999**, *55*, 961-967.
30. Cheng, Z. H.; Yasukawa, A.; Kandori, K.; Ishikawa, T., FTIR Study of Adsorption of CO_2 on Nonstoichiometric Calcium Hydroxyapatite. *Langmuir* **1998**, *14*, 6681-6686.